actuators

MDPI

Article

A Novel Two Stage Controller for a DC-DC Boost Converter to Harvest Maximum Energy from the PV Power Generation

Asma Charaabi [1], Oscar Barambones [2,*] and Abdelaziz Zaidi [1] and Nadia Zanzouri [1]

[1] LR11ES20 Laboratory of Analysis, Conception and Control of Systems, National Engineering School of Tunis, University of Tunis El Manar, Tunis 1002, Tunisia; Asma.Charaabi@enit.rnu.tn (A.C.); abdelaziz.zaidi@issatkr.u-kairouan.tn (A.Z.); Nadia.zanzouri@enit.rnu.tn (N.Z.)

[2] Department of Systems Engineering and Automation, Faculty of Engineering Vitoria-Gasteiz, University of the Basque Country (UPV/EHU), Nieves Cano 12, 01006 Vitoria-Gasteiz, Spain

* Correspondence: oscar.barambones@ehu.es

Received: 9 March 2020; Accepted: 10 April 2020; Published: 14 April 2020

Abstract: In this article, an efficient and fast two-stage approach for controlling DC-DC boost converter using non linear sliding mode controller for a PV power plant is proposed. The control approach is based on two online methods instead of using the conventional combination of online and offline methods to harvest maximum energy and deliver an output PV voltage with reduced ripples. The proposed two-stage maximum power point tracking (MPPT) control can be integrated into many applications such as hybrid electric vehicles. Simulation results compared with the standard approaches P&O prove the tracking efficiency of the proposed method under fast changing atmospheric conditions of an average 99.87% and a reduced average ripple of 0.06. The two-stage MPPT control was implemented involving the embedded dSPACE DSP in comparison to the classical P&O to prove the efficiency and the validity of the control scheme. The experimental set-up system was carried out on boost converter and programmable DC electronic resistive load to highlights the robustness of the proposed controller against atmospheric changes and parametric variation.

Keywords: non linear sliding mode; DC-DC boost converter; two-stage MPPT; PV power plant; MPPT

1. Introduction

Nowadays, due to the increasing global warming and the dropping of the conventional sources of fossil-fuel energy, renewable energy sources (solar, fuel cells, wind, etc.) continue presenting a sustained growth worldwide. Renewable energy minimizes the rising concern of global warming and CO_2 emissions, as well as mitigates the perilous effect on human health and the environment, which makes it very interesting for facilities in cities. Solar energy is considered to be an alternative energy source for expanded employment owing to its abundance and relatively free and easy access almost everywhere. Photovoltaic (PV) systems have been widely deployed in different applications [1–3]. Photovoltaic arrays produce electrical current from the solar irradiance; typically, they have a strong nonlinearity related to their power characteristic.

The power generator depends on the solar irradiation and temperature; a single operating point called the maximum power point (MPP) exists under certain conditions for each PV module. To eliminate the issue of mismatches occurring between the voltage and current characteristics of MPP and the load, we often connect a DC-DC converter at the output of the PV module. Indeed, the tracking of the MPP is very substantial not only to enhance the system's effectiveness, but also to decrease the number of solar panels needed for the desired output power, which helps reduce installation costs [4].

DC-DC converters are widely deployed in industrial and domestic application due to their simple design and implementation with low cost; howeverm many DC-DC converter topologies are adopted to be used in Stand-alone or grid-connected PV systems, such as: buck, boost, buck–boost, sepic, cuk, etc. The only drawback of using a buck or buck–boost converter is the discontinuous input current, which causes undesired oscillation that will deteriorate the MPPT efficiency while boost, sepic, and cuk converters with continuous input current only have an input current ripples [5].

Several MPPT algorithms have been proposed to overcome the waste of energy due to climate changes and the low efficiency of energy conversion. A review provides an update of the advanced and the conventional techniques with their benefits and drawbacks [6]. These techniques can be classified into two classes: offline and online methods. Offline methods generally utilize some solar array parameter values to produce the control sign needed for reaching MPP. These methods include short circuit current method [7] and open circuit voltage method [8].

The main advantage of these methods is their simplicity and the cost-effectiveness of implementation, since they only require one feedback loop. Nevertheless, the drawback appears in the computation of MPP, which is based on the estimation in the steady state and the power losses produced by the interruption of the system's operation to extract the value of the open-circuit voltage. Online methods are usually used for tracking real time MPP PV voltage and current values, and include the extremum seeking control method [9,10], perturb and observe method [11,12], and incremental inductance control [13,14]. The knowledge of the PV characteristics with this type of algorithm is not required, but the major problems are the failure to track the rapid weather changes and the slow convergence speed.Some new methods based on a combination between online and offline techniques, e.g., hybrid techniques [15] or maximum power voltage MPV, have been proposed to overcome the demerits of the previous methods [16,17]. In [18], a hybrid MPPT technique is used in combination with the open circuit voltage V_{oc} and the P&O algorithm. Despite the admissible behavior in some conditions, the offline methods are only suitable for temperature changes and fallible in the case of irradiance change. In [19], an improved MPPT controller based on two loop configuration is proposed. The Artificial Neural Network (ANN) generates the optimum maximum voltage of the PV system, and then a second loop using the classical P&O ensures the tracking of MPP. The efficiency of the proposed MPPT method was demonstrated through simulations and comparison with a conventional algorithm. In [20], a P&O method with variable size perturbation is used to extract the V_{MPP}, and then a fuzzy logic control FLC is used for tracking MPP. Jie et al. [21] demonstrated that the reference voltage extracted from P&O is improved compared to the classical duty ratio P&O. Simulation and experiments showed that the improved P&O minimized effectively power fluctuation in addition of high tracking efficiency under variable light intensity.

Generally, MPPT techniques have crucial characteristics such as convergence speed, accurate tracking, and computational complexity. It is realized that the combination of two MPPT algorithms overcomes the limitations of using individual MPPT techniques alone [22]. In fact, the online P&O algorithm offers an accurate tracking of the MPP with low complexity implementation. Many linear controllers can be associated with the P&O method to form a two-stage MPPT controller, which ensures a suitable tracking of the generated voltage reference to decrease the disturbances [23]. However, the main drawback of linear controllers is that they are developed based on a PV model around a given operating point, which leads to an unstable PV system. Therefore, the use of nonlinear controllers presents a good solution due to the strong nonlinearity of the PV panel and the power converter. Nonlinear sliding mode MPPT controller was proposed in [24] and compared with two conventional MPPT methods (P&O and Incremental inductance) to illustrate the effectiveness of the proposed SMC controller; however, this method is based on an individual MPPT technique, which offers only the feature of one controller.

Sliding mode control (SMC) represents a robust controller, which is widely used in many applications such as robotics, motor, actuator control, and photovoltaic energy field [25–27]. Its high performance and simplicity of implementation promote researchers to focus more on this controller

and prove its efficiency with real time experimental validation. The aim of this task is to create a further two-stage controller scheme based on the nonlinear sliding mode for DC-DC power converter. The control scheme contains two loops. The first loop is done based on perturb and observe algorithm to estimate the real time maximum power voltage MPV reference. The second one is to adjust the PV voltage to the estimated voltage reference. This method solves the divergence problem and reduces the steady state oscillations by applying a voltage estimator-based P&O that can be used in combination with either an MPPT method or nonlinear method such as SMC. Our main contributions using the two-stage MPPT method are: (a) the improvement of the settling time; (b) the elimination of overshoots and the reduction of undershoots; and (c) the reduction of ripple and thus an increase in the robustness and efficiency against parametric variation, which leads to harvesting the maximum energy from the PV system.

The remainder of the paper includes the following sections. The PV system model is provided in Section 2 including the model of the PV panel and the boost converter. In Section 3, the proposed scheme design of the control is developed. Afterwards, the instrumentation used in real time experiments are detailed in Section 4. Section 5 illustrates the simulation results of the controller compared with the P&O algorithm. Then, the experimental results and discussion are described in Section 6. Finally, Section 7 contains the conclusion and the perspectives of this work.

2. Photovoltaic System Model

The completed PV system model is illustrated in Figure 1 and is constituted by a PV array connected to resistive load through DC-DC boost converter. The description of each part is below.

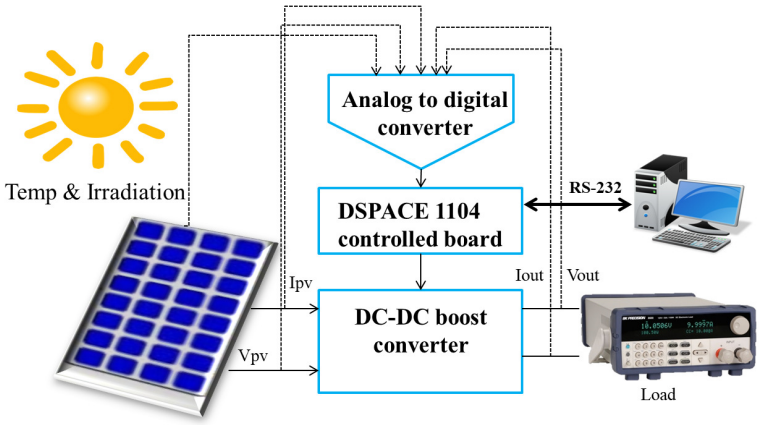

Figure 1. Structure of PV system.

2.1. Photovoltaic Cell Modeling

Photovoltaic cells absorb light energy using a semiconductor P-N junction and they are wired in different parallel and series combinations to establish a panel. The PV modules are assembled into PV arrays to generate a certain voltage/current levels. In [28–30], different solar cell models are presented. Due to the strong nonlinearity of the PV cell model, an electrical equivalent circuit model is commonly adopted [31]. The PV power and current are calculated with high precision using this model.

Figure 2 presents the electrical model of a solar cell, which contains a source of current in parallel with a diode and a parallel resistor R_p connected to a serial resistor R_s.

Resistances R_s and R_p can be neglected, due to the low and the high values, respectively, thus simplifying the study. Typical electrical (I–V) of a PV cell is given by the following equations [32], with the symbols illustrated in Table 1.

$$I_{pv} = N_p I_{ph} - N_P I_d \left[\exp\left(\frac{q v_{pv}}{N_s A k T_{ak}}\right) - 1\right] \quad (1)$$

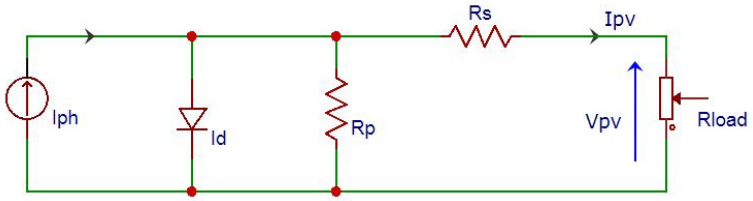

Figure 2. PV cell equivalent circuit model.

All other parameters of Equation (1) can be defined by:

$$\begin{cases} I_d = I_{rr}(\frac{T_{ak}}{T_{rk}})^3 \exp\left[(\frac{E_g q}{kA})(\frac{1}{T_{rk}} - \frac{1}{T_{ak}})\right] \\ I_{rr} = \frac{I_{scr}}{\left[\exp(\frac{qv_{oc}}{kN_S A T_{rk}})-1\right]} \\ I_{Ph} = I_{scr} + [K_i(T_{ak} - T_{rk})]\,\frac{s}{1000} \end{cases} \quad (2)$$

Table 1. Nomenclature.

Symbol	Definition
I_{ph}	Photo current [A]
I_d	Reverse saturation current [A]
A	Ideality factor
I_{scr}	Short circuit current [A]
v_{oc}	Open circuit voltage [V]
K_i	Temperature coefficient of short circuit current [A/K]
T_{ak}	Cell temperature [K]
T_{rk}	Cell reference temperature [K]
S	Solar irradiation [W/m^2]
K	Boltzmann constant, $K = 1.38 \times 10^{-23}$[J/K]
E_g	Band gap energy [eV]
q	Electron charge, $q = 1.6 \times 10^{-19}$[C]

2.2. The Boost Converter Model

To guarantee the extraction of the maximum power operating point, we must add a switch converter between a PV panel and a resistive load [33]. We need to get a higher regulated output voltage from the input voltage, which is why a DC-DC boost converter is required. The boost converter can work under two different cases regarding the current of the inductor I_L. The continuous conduction mode (CCM) occurs when I_L does not reach the zero value. The discontinuous conduction mode (DCM) happens when the frequency decreases or the output current I_0 is lower than the limit of the CCM switching.

The converter used in the real time application works in CCM and its typical topology is shown in Figure 3.

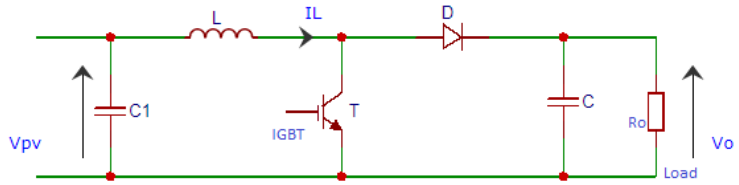

Figure 3. Boost converter topology.

The boost converter is a nonlinear and variable structure system. Referring to Asma et al. [34], the state space representation is defined by:

$$\begin{bmatrix} \dot{I}_L \\ \dot{V}_0 \end{bmatrix} = \begin{bmatrix} 0 & \frac{\alpha-1}{L} \\ \frac{1-\alpha}{C} & \frac{1}{R_0 C} \end{bmatrix} \begin{bmatrix} I_L \\ V_0 \end{bmatrix} + \begin{bmatrix} \frac{1}{L} \\ 0 \end{bmatrix} v \tag{3}$$

The system may be defined by the bilinear model: $\dot{x} = f(x) + g(x)u$

$$\begin{bmatrix} \dot{I}_L \\ \dot{V}_0 \end{bmatrix} = \begin{bmatrix} \frac{V_{pv}}{L} - \frac{V_0}{L} \\ \frac{I_L}{C} + \frac{V_0}{R_0 C} \end{bmatrix} + \begin{bmatrix} \frac{V_0}{L} \\ -\frac{I_L}{C} \end{bmatrix} \alpha \tag{4}$$

where

$$f(x) = \begin{bmatrix} \frac{1}{L}(V_{pv} - V_0) \\ \frac{1}{C}(I_L - \frac{V_0}{R_0}) \end{bmatrix}, \; g(x) = \begin{bmatrix} \frac{V_0}{L} \\ -\frac{I_L}{C} \end{bmatrix} \; and \; u = \alpha \tag{5}$$

The relation between the input and the output voltage is directly proportional to the duty ratio α.

$$V_0 = \frac{V_{pv}}{1-\alpha} \tag{6}$$

Based on the assumption of no loss in the circuit elements $P_{pv} = P_0$, the power delivered to the load must be the same as the power supplied by the photovoltaic module:

$$P_{pv} = P_0 \Rightarrow V_{pv} I_{pv} = V_0 I_0 \tag{7}$$

Substituting Equation (7) into Equation (6) yields:

$$I_0 = I_{pv}(1-\alpha) \tag{8}$$

With the resistance load $R_0 = V_0 / I_0$, we obtain:

$$R_0 = \frac{R_{pv}}{(1-\alpha)^2} \tag{9}$$

3. Control Design of The Proposed Two-Stage MPPT Algorithm

We propose a two-stage method for MPPT to respond to the objective of good output accuracy and robustness against weather changing. The control structure scheme is given by Figure 4. The control design consists of two steps: the first one corresponds to estimating the MPV voltage and the second is for tracking. I_{pv} and V_{pv} values are measured from PV module and sent to MPPT searching algorithm to provide the maximum power voltage reference V_{pvd}. Afterwards, the sliding mode controller SMC tracks this reference.

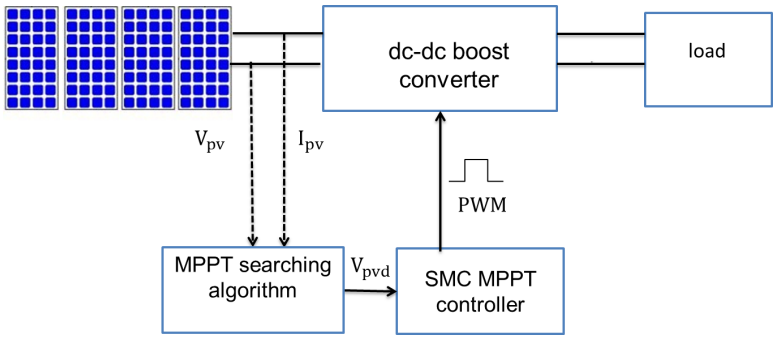

Figure 4. Controller design.

3.1. MPP Searching Algorithm

To estimate the real time MPV reference, we employ the P&O algorithm [35]. This method is widely used for MPP tracking because of its simple structure and few variables required in the implementation. The strategy of this algorithm is based on the slight variation (perturb) in voltage ΔV_{pv} through the converter duty ratio α. Then, ΔP_{pv} is measured. If $\Delta P_{pv} > 0$, the working point of the PV module is nearer to MPP and the following variation takes place in the same trend as the preceding one; otherwise, if $\Delta P_{pv} < 0$, the obtained operating point of the system is far from MPP and the following variation occurs in the contrary direction. The variation is carried out through the duty cycle α. Referring to Equation (9), an increment of α leads to a decrease of the input resistance R_{pv}, hence a decrease in the operating voltage V_{pv} (and vice versa).

The process is repeated until attaining MPP. Afterwards, the system operates around that MPP. The algorithm summary behavior is illustrated in Table 2.

Table 2. Behavior of P&O algorithm.

Measurements	Voltage V_{pv}	Duty Cycle (α)
$\Delta P_{pv} > 0, \Delta V_{pv} > 0$	Rise	Drop
$\Delta P_{pv} > 0, \Delta V_{pv} < 0$	Drop	Rise
$\Delta P_{pv} < 0, \Delta V_{pv} < 0$	Rise	Drop
$\Delta P_{pv} < 0, \Delta V_{pv} > 0$	Drop	Rise

We analyze the four cases behaviors for the photovoltaic panel to follow MPP:

- Case 1: $\Delta P_{pv} = P_{pv}(k) - P_{pv}(k-1) > 0$, $\Delta V_{pv} = V_{pv}(k) - V_{pv}(k-1) > 0$

ΔP_{pv} is the difference of the present power $P_{pv}(k)$ minus the previous $P_{pv}(k-1)$ and ΔV_{pv} is also the gap among the actual PV voltage $V_{pv}(k)$ and the previous one $V_{pv}(k-1)$. In Case 1, both ΔP_{pv} and ΔV_{pv} are positive. Therefore, the algorithm decreases the duty cycle α so that V_{pv} continues to rise to reach MPP.

- Case 2: $\Delta P_{pv} = P_{pv}(k) - P_{pv}(k-1) > 0$, $\Delta V_{pv} = V_{pv}(k) - V_{pv}(k-1) < 0$

Here, ΔP_{pv} is positive while ΔV_{pv} is negative; referring to Figure 5, the PV module is working in the right of MPP. The algorithm's action is to decrease the PV voltage by increasing the duty cycle α until MPP is reached.

- Case 3: $\Delta P_{pv} = P_{pv}(k) - P_{pv}(k-1) < 0$, $\Delta V_{pv} = V_{pv}(k) - V_{pv}(k-1) < 0$

In this case, both ΔP_{pv} and ΔV_{pv} are negative. The control decision is to reduce the duty cycle α to raise the PV voltage until reaching MPP.

- Case 4: $\Delta P_{pv} = P_{pv}(k) - P_{pv}(k-1) < 0$, $\Delta V_{pv} = V_{pv}(k) - V_{pv}(k-1) > 0$

In the last case, ΔP_{pv} is negative while ΔV_{pv} is positive. The decision assumed is to increase the duty ratio to lead the decreasing of the PV voltage V_{pv}.

3.2. Sliding Mode Controller

The function of the SMC is to regulate the voltage generated by the photovoltaic panel V_{pv} at a reference value V_{ref} estimated by the MPP searching algorithm. The switching function can be chosen as follows:

$$s = V_{ref} - V_{pv} \tag{10}$$

Referring to the general form of Equation (5) and using the equation $\dot{s} = 0$, we obtain the equivalent control u_{eq} that leads the system to the manifolds.

$$\dot{s} = \frac{\partial s}{\partial x} \cdot \frac{\partial x}{\partial t} = s_x(x) \cdot (f(x) + g(x) \cdot u_{eq}) = 0 \tag{11}$$

By solving this equation:

$$u_{eq} = -\frac{s_x\, f(x)}{s_x\, g(x)} = 1 - \frac{V_{pv}}{V_0} \tag{12}$$

To prove the stability of our controller, we use the Lyapunov theory. This function can be taken as follows:

$$V = \frac{1}{2}s^2 \tag{13}$$

Its derivative is given by:

$$\dot{V}(x) = s\frac{\partial s}{\partial t} = s\dot{s} \tag{14}$$

Applying this function on the switching surface:

$$\begin{aligned} s &= e = V_{ref} - V_{pv} \\ \dot{s} &= \dot{e} = -\dot{V}_{pv} \end{aligned} \tag{15}$$

- **When s $>$ 0:** This denotes that the voltage reference V_{ref} provided by the MPP searching algorithm based on P&O is bigger than the PV voltage of the PV module, i.e., $V_{ref} > V_{pv}$. Afterwards, this leads s to zero $(s = 0)$, meaning $(V_{pv} = V_{ref} = V_{MPP})$. As shown in Figure 5, V_{pv} should increase and I_{pv} should decrease; therefore, as a result, R_{pv} must increase through decreasing the duty cycle α, which is deduced from Equation (9).
  As a conclusion, the system is stable when V_{pv} is increased, which implies that $\dot{s} = -\dot{V}_{pv} < 0$, then $s\dot{s} < 0$, and our system moves toward the maximum power point.
- **When s $<$ 0:** Based on Equation (10), $(V_{pv} > V_{ref})$; thus, to stabilize our system $(s = 0)$ and according to Figure 5, V_{pv} must decrease and I_{pv} should increase. Therefore, R_{pv} has to drop, which occurs through raising the duty ratio α, denoting that $\dot{s} = -\dot{V}_{pv} > 0$ and $s\dot{s} < 0$.
  Finally, based on Lyapunov stability theory, we deduce that the control law is stabilizing.

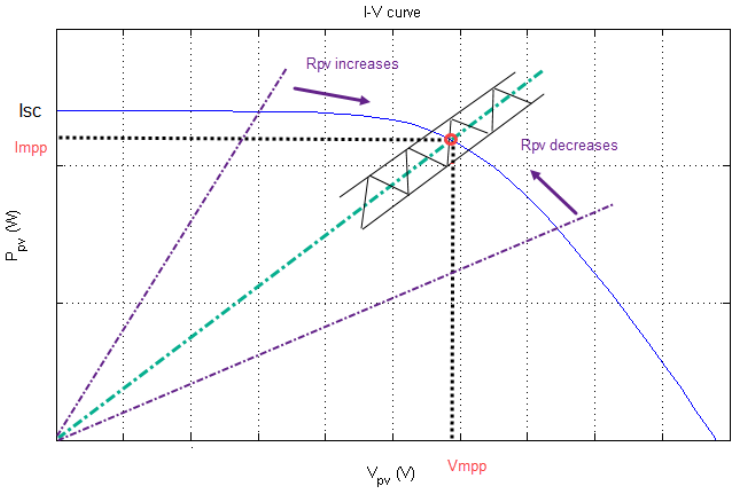

Figure 5. I–V characteristic curve.

4. Instrumentation Used in Real Time Experiments

The real PV system is comprised of:

1. Four PV panels connected in parallel and their specifications are presented in Table 3.
2. A DSP1104.
3. A boost converter with specifications given in Table 4.
4. A programmable DC Electronic loads model 8600 BK Precision.

4.1. Atersa PV Panel

Table 3 presents the characteristics of the Atersa PV panel.

Table 3. Characteristics of Atersa A-55 PV panel.

Parameter	Value
Power (W in test ±10%)	55 W
N_s	36
I_{mp}	3.4 A
V_{mp}	16.2 V
I_{sc}	3.7 A
V_{oc}	20.5 V
Temperature coefficient of I_{sc}	1.66 mA/ C
Temperature coefficient of V_{oc}	−84.08 mV/ C

4.2. Boost Converter

The corresponding technical specifications are summarized in Table 4.

Table 4. Boost converter parameters.

Parameter	Type	Value
L	6xPCV-2-564-08	560 µH, 7 A, 42 m Ω
C	2xTK Series	1500 µF, 250 V
C_1	1xTK	1000 µF, 250 V
Schottky diode	2xMURF1560GT	600 V, 15 A, 0.4 V
IGBT	1xHGT40N60B3	600 V, 40 A, 1.5 V
F_s		20 KHz
V_{imax}		60 V
I_{imax}		20 A
V_{Omax}		250 V
I_{Omax}		20 A
α_{min}		0.1
α_{max}		0.9

4.3. DSP1104

The Digital Signal Processors (DSP) controller is a strong device for fast control systems. It presents a perfect solution in industrial fields. Figure 6 summarizes the components required for application.

1. **Matlab/Simulink and Control Desk** :
   The software packages used in the experimental test are Matlab-Simulink and Control Desk 5.1. Indeed, the way we made our control strategies is the same as making any Simulink project, by using basics blocs or toolboxes via installing the library RTI 1104 in Simulink-Matlab. Thereafter, we compiled the Simulink model and generated a (.sdf) file, which is a specific code in real time. Control Desk 5.1 is wasused for creating an interface with the GUI (graphical user interface). Figure 6 illustrates how the real-time code is obtained from (.sdf) file generated from Simulink, which allows us to access and modify the variable control system in real time.
2. **I/O ribbon cable** :
   It is used to connect the DS1104 R&D controller card to the I/O box.
3. **CP 1104 I/O box** :
   It is an input/output interface board between the DS1104 R&D controller board and the system. It contains eight analog input digital converters (ADCs), eight analog output digital converters, and two digital input incremental encoders.

4. **DS1104 R&D controlled board**:
This board is installed in the computer and connected to the CP 1104 I/O through a master I/O ribbon cable. The DS1104 runs with Power PC 603e core at 250 MHz with 32 MB of SDRAM and 8 MB of flash memory.

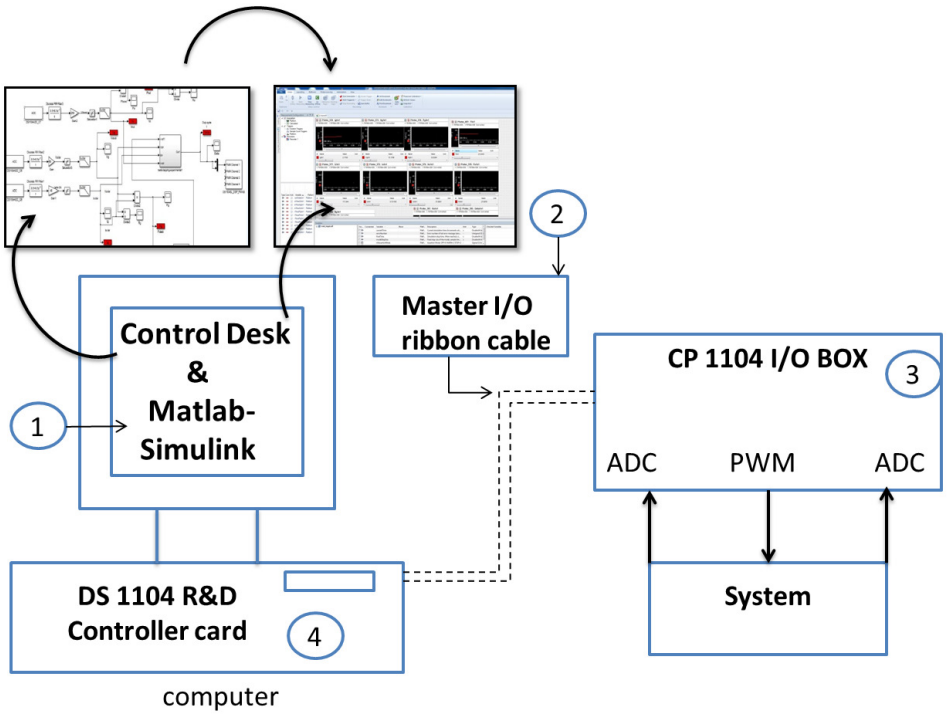

Figure 6. Components of the application.

5. Simulation Results

The two-stage MPPT algorithm was compared with the P&O method and both were created by SIMSCAPE library of the environment Matlab/Simulink software. To test the proposed controller more effectively in a realistic environment, real power electronics switching devices, with forward voltage drops and resistances, were considered for simulation tests. More details about the effects of parasitic components on the dynamic response of power converters are underlined in the following subsection.

5.1. Effects of Parasitic Components

The effect of parasitic elements on the modeling of DC-DC power converter is very substantial. However, its impact is observed especially on the energy losses. In the literature, many studies [36–39] are focused on the analysis and the modulation of non-ideal DC-DC power converter operating on the discontinuous conduction mode DCM and the continuous conduction mode CCM. Reatti et al. [39] presented nonlinear models of both buck and boost converters for the ideal case (without parasitic) and the non-ideal case (with parasitic) operating on the CCM. This comparison underlines the impact of the parasitic components on the transient and steady state response. In [37], a comparison between two modeling techniques suitable for DCM of DC-DC converter taking into account the parasitic components is presented. This comparison shows that the small-signal equivalent circuit allows a fast and accurate frequency domain analysis. An improved average cell modeling including the effect of parasitics on inductor current is proposed in [36]. The proposed model improves several existing models in both time and frequency domains. Locorotondo et al. [38] focused in the effect of parasitic elements of the MOSFET component of DC-DC converter regarding the effect of nonlinear junction capacitances and the stray inductances in terms of overshoot, ringing, and energy losses.

Therefore, the model of the DC-DC boost converter was made using the SIMSCAPE library, which provides a more realistic modeling of physical components taking into account the following parasitic components. the on-resistance of the IGBT switching device $r_s = 0.1\ \Omega$ with forward voltage drops $V_{fd} = 0.7\ V$; the parasitic resistance of the inductor $r_l = 42\ m\Omega$ else; the on-resistance of diode $r_d = 0.001\ \Omega$; and the diode threshold voltage $V_F = 0.7\ V$.

Nevertheless, to avoid the problem of the infinite output voltage at d=1, the duty cycle is limited to 0.1- 0.9 in our control scheme because these are the admissible values for our real DC-DC converter.

In real time tests, it is impossible to impose weather conditions while in the simulations it is easy to choose any weather condition. Therefore, in these simulations, we observes the behavior of each controller under brusque changes of irradiance and temperature and analyzed the ability of the controllers to force the photovoltaic system to track MPP. Simulations were performed for two possibilities: a simulation at inconstant irradiance and steady temperature and a simulation at steady irradiance and inconstant temperature.

5.2. Simulation under Steady Temperature

This test was carried out at steady temperature $T = 25\ ^{\circ}C$ and for fast irradiance change. It started from 700 W/m^2 for 1 s and it decreases quickly to 400 W/m^2 over 1 s.

Figure 7 shows the PV output power response of the two-stage MPPT controller compared with the response of the P&O method under fast irradiance change. In this figure, we can see clearly that the overshoot of the proposed controller is almost negligible on both irradiance levels (0.12 and 0.026 W); similarly, for the P&O method, it is equal to 0.17 and 0.55 W. However, the P&O method presents a significant undershoot on the first level of irradiance equal to 30.54 W while an insignificant overshoot for the two-stage MPPT method is noticed. Moreover, the proposed method converges rapidly to MPP with a settling time around 61 and 0 ms against an important settling time of the P&O around 241 and 472 ms. To further analyze the performances of the two controllers in steady state, the ripple of the PV output power is presented on each level of irradiance. The two-stage MPPT method shows a good performance with less ripple around 0.098 and 0.001 against 0.313 and 0.011 for the P&O algorithm.

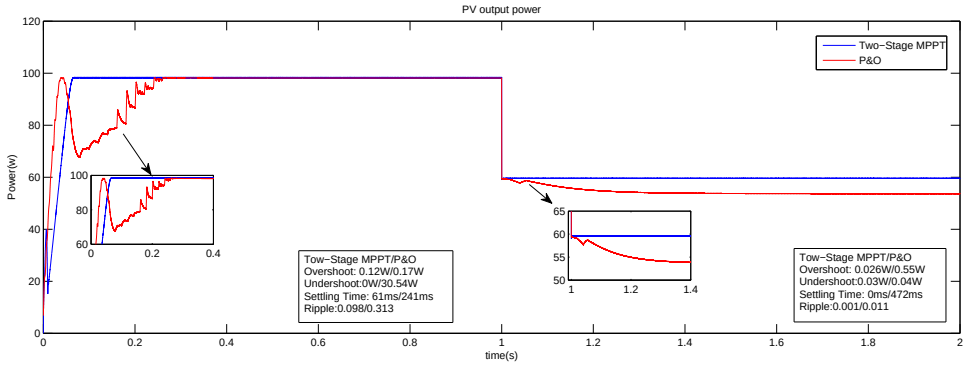

Figure 7. PV output power under irradiance changes.

Figure 8 presents a comparison between the load power of the two-stage MPPT and the conventional P&O algorithm. From the comparison below, it is clear that the proposed controller outperform the P&O MPPT by transmitting further maximum power load under fast irradiation change within settling time around 221 and 181 ms. However, some ripple and oscillation are noticed in the dynamic response of the load power around 0.106 and 0.063. The P&O method harvests less power load with longer settling time compared with the two-stage method (271 and 333 ms). In addition, ripple and oscillation around the steady state power load are noticed (0.107 and 0.09).

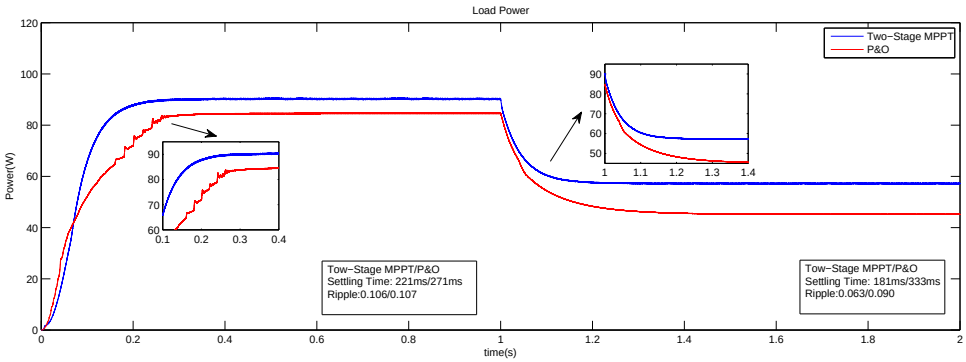

Figure 8. Load power under irradiance changes.

5.3. Simulation at Steady Irradiation

In this test, the solar irradiance remained constant at S = 600 W/m^2 while the temperature started at 45 °C within 1 s and then decreased to 20 °C for 1 s.

The behavior of both MPPT controller is depicted in Figure 9. As can be observed during the transient response at 45 °C , a ripple around 0.283 is noticed using the P&O method against almost negligible ripple using the two-stage method of around 0.096. However, we can also see a significant undershoot of the P&O method equal to 21.22 W while no over- or undershoot is observed in the behavior of the proposed method. In addition, both methods can achieve MPP within settling time around 54 and 240 ms for the proposed method and the P&O method, respectively.

At the low temperature of 20 °C , the proposed approach rapidly tracks MPP with settling time equal to 8 ms with no overshoot, no undershoot, and a negligible ripple (0.015), whereas the P&O method tracks the MPP with a bigger settling time around 216 ms compared with the two-stage method, with a steady state error and undershoot equal to 1.14 W.

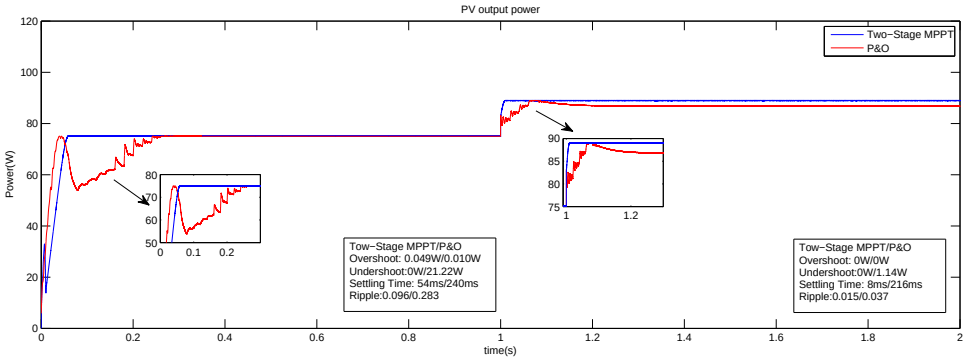

Figure 9. PV output power under temperature changes.

The dynamic response of the load power for both controllers is presented in Figure 10. Clearly, from the simulation results the two-stage MPPT approach can transfer more maximum power to the load under the temperature variation with fast settling time (210 and 218 ms) compared with the P&O algorithm, which transmits less maximum power to the load with settling time around 259 and 258 ms. However, the two-stage MPPT controller presents some ripple around 0.107 and 0.020 against 0.104 and 0.018 for the conventional P&O algorithm.

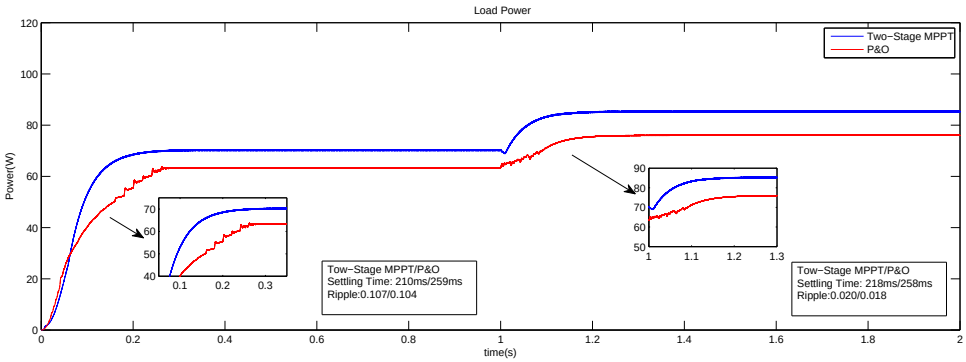

Figure 10. Load power under temperature changes.

As a conclusion, our proposed algorithm is proven from the two tests, namely simulation under fast variation of irradiance and simulation under fast temperature change, by outperforming the conventional P&O method, improving the settling time with almost negligible under- and overshoot and decreasing the ripple. Table 5 summarizes the results provided by simulation tests. The tracking efficiency and the error tracking for each controller is presented.

The equation of the tracking efficiency and the tracking error are defined as follow:

$$Efficiency = \frac{P_{pv}}{P_{MPP}} \times 100\% \tag{16}$$

$$Error = \frac{P_{MPP} - P_{pv}}{P_{MPP}} \times 100\% \tag{17}$$

Table 5. Performances of controllers.

	Settling Time 2%		Overshoot		Ripple		Efficiency		Error	
	P&O	**Two-Stage MPPT**	**P&O**	**Two-Stage MPPT**	**P&O**	**Two-Stage MPPT**	**P&O**	**Two-Stage MPPT**	**P&O**	**Two-Stage MPPT**
					Fast irradiance variation (W/m^2): from (1):S=700 to (2): S=400					
(1)	241 ms	61 ms	0.17 W	0.12 W	0.313	0.098	99.87	99.97	0.12	0.02
(2)	472 ms	0 ms	0.55 W	0.02 W	0.011	no ripple	90.26	99.92	9.73	0.08
					Fast temperature variation(°C) from (1):T=45 to (2): T=20					
(1)	240 ms	54 ms	0.01 W	0.04 W	0.283	0.096	99.89	99.89	0.106	0.106
(2)	216 ms	8 ms	2.15 W	0 W	0.037	0.015	97.72	99.80	2.273	0.191

6. Experimental Results and Discussion

Figure 11 shows a part of instrumentation used in experiments.The real PV system components are: PV panel, a DSP real time controller board, a programmable DC electronic loads, a boost converter, and a computer to store the measured data. Experiments of the two algorithms (two-stage MPPT and P&O) ran in Simulink/Matlab, as shown in Figure 12, and using the card, which is known with its capability of integration in Simulink.

Implementation in Simulink was performed using some elements from the 1104 library:

- DS1104_Mux_ADC DS1104: This block is for reading the four A/D converter channels. The two algorithms only need the irradiation (G) and the temperature (T) at every sample time.
- DS1104_ADC_CX: It is devoted to reading the data of the four signals from (ADC_C5 to ADC_C8). ADC_C5 is dedicated to reading the photovoltaic voltage (V_{Solar}=V_{pv}), ADC_C6 to reading the photovoltaic current (I_{Solar}=I_{pv}), ADC_C7 to V_O, and ADC_C8 to I_O.

- DS1104SL_DSP_PWM3: It allows generating standard PWM pulses.
- Low pass filters: They are used to remove the undesirable high-frequency noise.

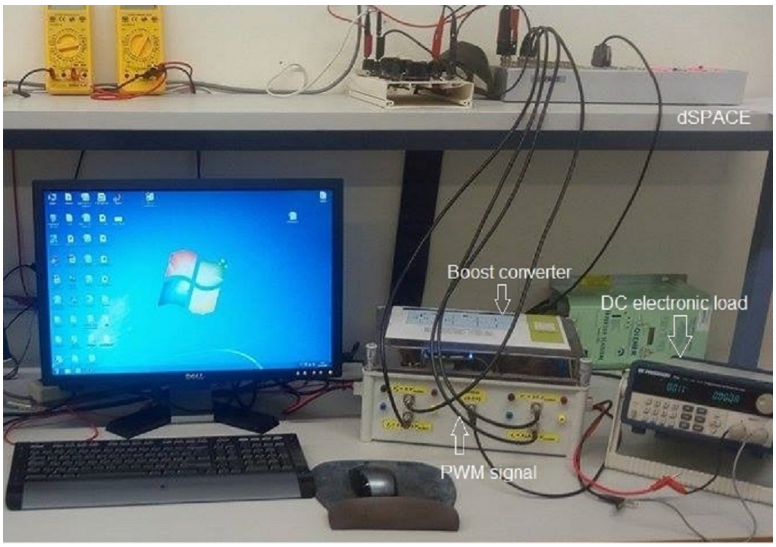

Figure 11. The real system.

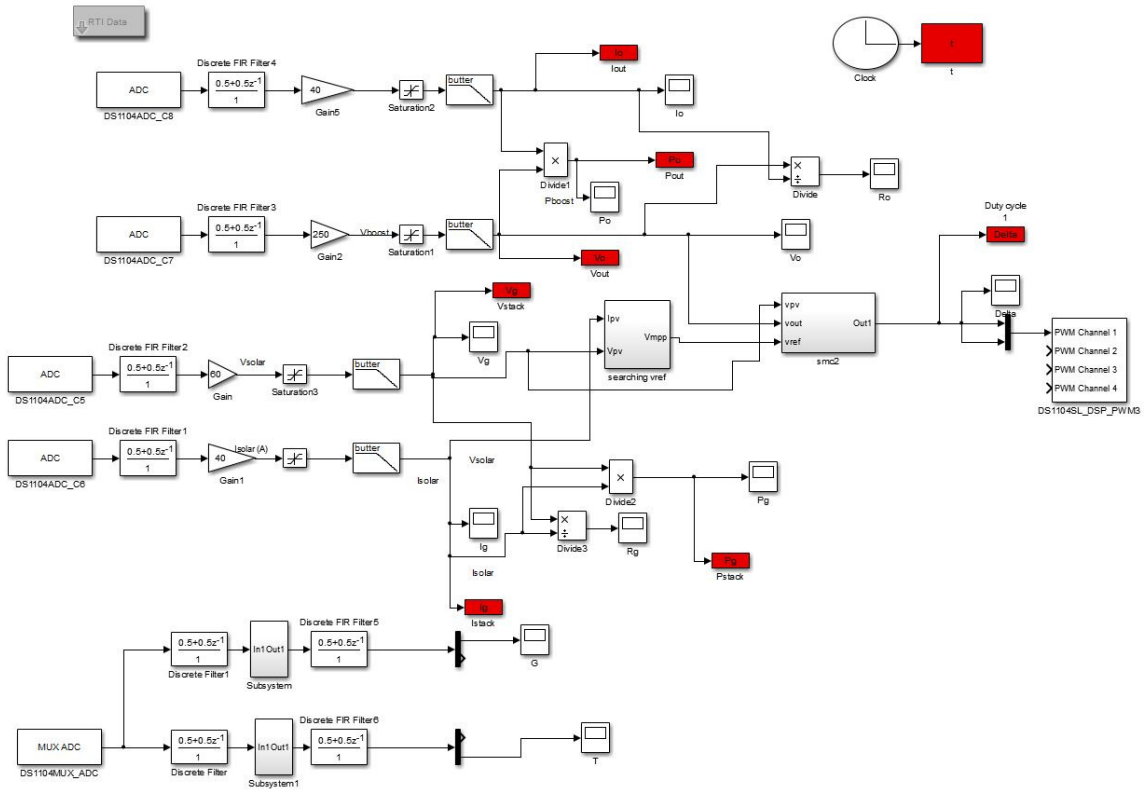

Figure 12. Simulink model of two-stage MPPT control.

The experiments were carried out in the same way for the two algorithms and the analysis of the behavior for each algorithm was performed under abrupt change in the resistance load from two values using the programmable 8600 BK DC electronic load. In fact, many features are provided by this type of load instead of the traditional and manual resistive load, among them: a flexible operation mode constant current (CC), resistance (CR), voltage (CV), and power (CP). Resistance/power or

voltage/current values were measured and displayed in real time with high resolution. The protection of the real system could be guaranteed (over-current or over-voltage) and the greatest benefit is that it generated a list mode resistance waveform sequences with rapid, accurate resistance values and precise timing.

For each test, we calculated the maximum power that we should obtain from the PV panel using its characteristic curves: The first step was sending a command signal to DSP to generate a duty cycle equal to zero ($\alpha = 0$). The second step was to change the load resistance from 0Ω to the maximum resistance value in order to allow the system to go from $(I_{sc})(R = 0\ \Omega)$ to $(V_{oc})(R = 200\ \Omega)$.

6.1. Perturbation and Observation Algorithm

The weather conditions were the temperature of 22 °C and the irradiation of 155 W/m^2.

The obtained results correspond to sudden load resistance variation. It started from the value of 40 Ω, decreased to 30 Ω, and then rose to 50 Ω.

The real behaviors of the photovoltaic output power P_{pv}, the load power P_o, the PV voltage V_{pv}, and the load voltage V_o using the P&O method are presented in Figure 13. it is clear from the response of the PV output power P_{pv} that the P&O can track the maximum power point under load variation. However, an undershoot of 2.13 W and ripple of 0.12 around MPP are noticed. Similarly, for the load power, it presents two significant overshoots around 6.69 and 2.06 W, as well as two other undershoots equal to 4.24 and 7.43 W with ripple around 0.24. The impact of the variation load can be observed from the dynamic response of the load voltage V_o, which presents an overshoot of 3.13 V and an undershoot of 3.73 V with some ripple around 0.13. In addition, from the response of the PV voltage, an overshoot and an undershoot of around 1.61 and 1.36 V are noticed, respectively. Otherwise, oscillation and ripple (0.2) around the signal of PV voltage are present.

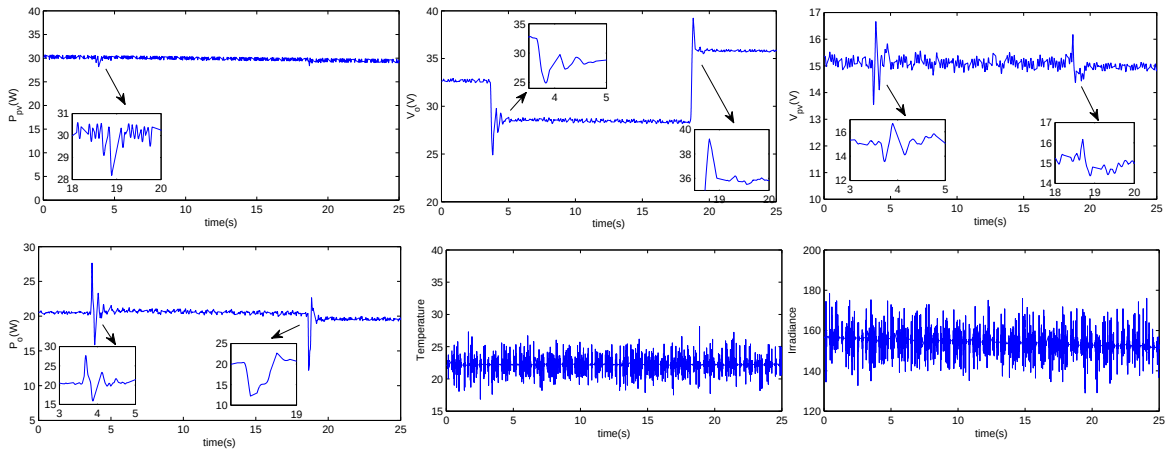

Figure 13. Real behaviors of P_o, P_{pv}, V_o, and V_{pv} using P&O algorithm.

6.2. Two-Stage MPPT Control

The weather condition was S = 231 W/m^2 and T = 23 °C . The real test was carried out under a variable resistance load. It started from a value of $R_o = 30\ \Omega$, increased to 50 Ω, and then decreased again to 40 Ω.

Figure 14 illustrates the real behavior of the PV output power P_{pv}, the load power P_o, the PV voltage V_{pv}, and the load voltage V_o using the two-stage MPPT controller. The two-stage method shows a significant improvement during the test and this can be observed in the behavior of the PV output power, which reaches MPP with no over- or undershoot as well as with less ripple of 0.07. Similarly, the proposed controller enhances the behavior of the PV voltage compared with the P&O algorithm since it has decreases the oscillation to 0.1 and increases the robustness by removing any over- or undershoot. Meanwhile, one overshoot is noticed in the response of the load power equal to

5.2 W with some ripple around 0.06. Moreover, the load voltage shows the impact of the resistance load change by following the same evolution with some ripple (0.04) and less overshoot (2.18 V).

The experimental tests confirm the simulation results, which accord that the two-stage MPPT method ensures a prompt convergence to the MPP with high accuracy by reducing the oscillation and ripple around MPP, which leads to harvesting the maximum energy from the PV panel. Furthermore, the proposed method shows an insensibility regarding the fast variation in weather condition by reducing the overshoots and the undershoots, and this reveals the robustness of our controller.

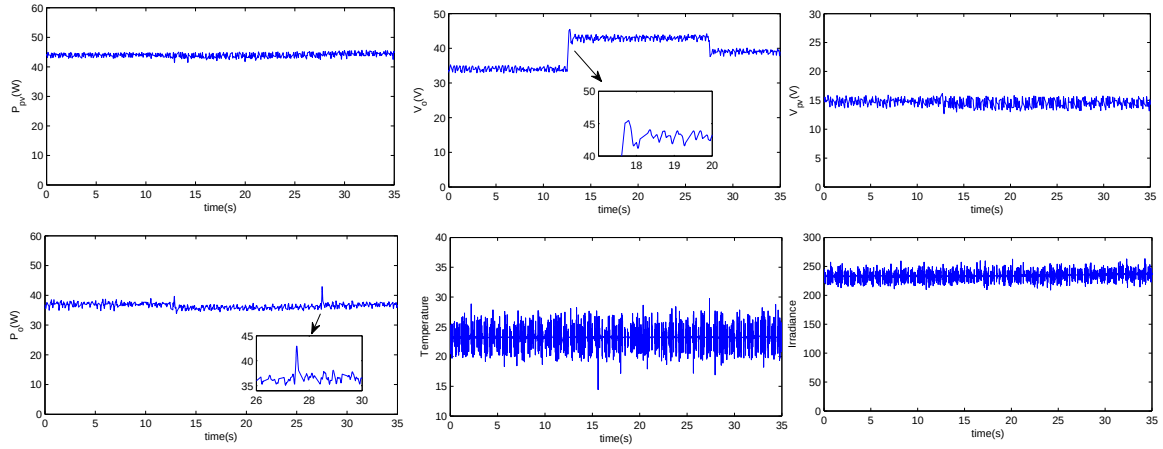

Figure 14. Real behaviors of P_{pv}, P_{Load}, V_{Load}, and V_{pv} using two-stage MPPT control.

7. Conclusions and Perspectives

In this article, a robust two-stage maximum power point tracking method for controlling a DC-DC boost converter through a regulated duty cycle to maximize the power delivered by a PV system is presented. Our method is composed of two steps, namely a maximum voltage estimator based on P&O and a fine-tune step using the nonlinear sliding mode controller.

Among the benefits of this development approach, it raises the stability of steady state with less ripple and ameliorates the rapidity of the transient tracking. The main idea of this controller is that it detects the variations in the parametric system, temperature, and solar irradiance by estimating the MPP in the first step. Then, it modifies the duty ratio of the boost converter by utilizing the sliding mode controller. This ensures a rapid convergence to the estimated voltage without oscillations.

The proposed method was compared with the standard P&O method through simulation tests under fast irradiance change and variable temperature. All the performance data of each method are summarized in a table to reveal the feature of the proposed approach. This performance data demonstrate that the two-stage method has a fast settling time less than 61 ms, less overshoot (<0.12 W), a reduced ripple (<0.09) with high average tracking efficiency around 99.87%, and an average tracking error of 0.09%. The two-stage MPPT controller was also validated by experimental tests to confirm the results obtained by simulation. The outcome of the comparison with the P&O reveals that the two-stage method is more robust on reacting against load resistance variation by removing the over- and undershoots from the PV output power. It also ensures convergence to the MPP with less ripple.

Our future work will be focused on energy management by insertion of a second source and the reliability improvement of the plant by replacing the conventional boost converter by an interleaved one.

Author Contributions: Conceptualization, A.C.; methodology, A.C.; software, A.C.; validation, A.C., O.B., A.Z., and N.Z.; formal analysis, A.C.; investigation, A.C.; resources, O.B.; data curation, A.C.; writing–original draft preparation, A.C.; writing—review and editing, A.C., O.B., A.Z., and N.Z.; visualization, A.C.; and supervision, O.B., A.Z., and N.Z. All authors have read and agreed to the published version of the manuscript.

Funding: This research received no external funding

Acknowledgments: The authors wish to express their gratitude to the Basque Government through the project SMAR3NAK (ELKARTEK KK-2019/00051), to the Diputación Foral de Álava (DFA) through the project CONAVAUTIN 2, and to the UPV/EHU for supporting this work, as well as to the Tunisian Government for supporting this work through the research lab LR11ES20.

Conflicts of Interest: The authors declare no conflict of interest.

Abbreviations

The following abbreviations are used in this manuscript:

MPPT	Maximum power point tracking
PV	Photovoltaic
MPP	Maximum power point
P&O	Perturbation and observation
DSP	Digital signal processor
MPV	Maximum power voltage
FLC	Fuzzy logic control
SMC	Sliding mode control
ADC	Analog to Digital Converter
DAC	Digital to Analog Converter

References

1. Kaushika, N.D.; Mishra, A.; Rai, A.K., Introduction to Solar Photovoltaic Power. In *Solar Photovoltaics: Technology, System Design, Reliability and Viability*; Springer International Publishing: Cham, Germany; New Delhi, India, 2018; pp. 1–14.
2. Nema, P.; Nema, R.; Rangnekar, S. A current and future state of art development of hybrid energy system using wind and PV-solar: A review. *Renew. Sustainable Energy Rev.* **2009**, *13*, 2096–2103. [CrossRef]
3. Sandelic, M.; Sangwongwanich, A.; Blaabjerg, F. Reliability Evaluation of PV Systems with Integrated Battery Energy Storage Systems: DC-Coupled and AC-Coupled Configurations. *Electronics* **2019**, *8*, 1059. [CrossRef]
4. Eccher, M.; Salemi, A.; Turrini, S.; Brusa, R. Measurements of power transfer efficiency in CPV cell-array models using individual DC–DC converters. *Appl. Energy* **2015**, *142*, 396–406. [CrossRef]
5. Valencia, P.A.O.; Ramos-Paja, C.A. Sliding-Mode Controller for Maximum Power Point Tracking in Grid-Connected Photovoltaic Systems. *Energies* **2015**, *8*, 12363–12387. [CrossRef]
6. Singh, O.; Gupta, S.K. A review on recent Mppt techniques for photovoltaic system. In Proceedings of the 2018 IEEMA Engineer Infinite Conference (eTechNxT), New Delhi, India, 13–14 March 2018; pp. 1–6.
7. Subudhi, B.; Pradhan, R. A comparative study on maximum power point tracking techniques for photovoltaic power systems. *IEEE Trans. Sustainable Energy* **2013**, *4*, 89–98. [CrossRef]
8. Bendib, B.; Belmili, H.; Krim, F. A survey of the most used MPPT methods: Conventional and advanced algorithms applied for photovoltaic systems. *Renew. Sustainable Energy Rev.* **2015**, *45*, 637–648. [CrossRef]
9. Munteanu, I.; Bratcu, A.I. MPPT for grid-connected photovoltaic systems using ripple-based Extremum Seeking Control: Analysis and control design issues. *Sol. Energy* **2015**, *111*, 30–42. [CrossRef]
10. Twaha, S.; Zhu, J.; Maraaba, L.; Huang, K.; Li, B.; Yan, Y. Maximum Power Point Tracking Control of a Thermoelectric Generation System Using the Extremum Seeking Control Method. *Energies* **2017**, *10*, 2016. [CrossRef]
11. Ishaque, K.; Salam, Z.; Lauss, G. The performance of perturb and observe and incremental conductance maximum power point tracking method under dynamic weather conditions. *Appl. Energy* **2014**, *119*, 228–236. [CrossRef]
12. Basha, C.H.; Rani, C. Different Conventional and Soft Computing MPPT Techniques for Solar PV Systems with High Step-Up Boost Converters: A Comprehensive Analysis. *Energies* **2020**, *13*, 371. [CrossRef]
13. Safari, A.; Mekhilef, S. Simulation and hardware implementation of incremental conductance MPPT with direct control method using cuk converter. *IEEE Trans. Ind. Electron.* **2011**, *58*, 1154–1161. [CrossRef]

14. Sivakumar, P.; Kader, A.A.; Kaliavaradhan, Y.; Arutchelvi, M. Analysis and enhancement of PV efficiency with incremental conductance MPPT technique under non-linear loading conditions. *Renew. Energy* **2015**, *81*, 543–550. [CrossRef]
15. Yang, C.Y.; Hsieh, C.Y.; Feng, F.K.; Chen, K.H. Highly efficient analog maximum power point tracking (AMPPT) in a photovoltaic system. *IEEE Trans. Circuits Syst. Regul. Pap.* **2012**, *59*, 1546–1556. [CrossRef]
16. Koizumi, H.; Kurokawa, K. A novel maximum power point tracking method for PV module integrated converter. In Proceedings of the IEEE 36th Power Electronics Specialists Conference, Recife, Brazil, 16 June 2005; pp. 2081–2086.
17. Jain, S.; Agarwal, V. A new algorithm for rapid tracking of approximate maximum power point in photovoltaic systems. *IEEE Power Electron. Lett.* **2004**, *2*, 16–19. [CrossRef]
18. Moradi, M.H.; Reisi, A.R. A hybrid maximum power point tracking method for photovoltaic systems. *Sol. Energy* **2011**, *85*, 2965–2976. [CrossRef]
19. Younis, M.A.; Khatib, T.; Najeeb, M.; Ariffin, A.M. An improved maximum power point tracking controller for PV systems using artificial neural network. *Przegląd Elektrotechniczny* **2012**, *88*, 116–121.
20. D'Souza, N.S.; Lopes, L.A.; Liu, X. Comparative study of variable size perturbation and observation maximum power point trackers for PV systems. *Electr. Power Syst. Res.* **2010**, *80*, 296–305. [CrossRef]
21. Dong, J.; Zhang, C,; Li, Y. Comparison of duty ratio perturbation & observation and reference voltage perturbation & observation methods applied in MPPT. In Proceedings of the 7th International Power Electronics and Motion Control Conference (IPEMC), Harbin, China, 2–5 June 2012; Volume 2, pp. 1358–1362.
22. Al-Soeidat, M.R.; Cembrano, A.; Lu, D.D. Comparing effectiveness of hybrid mppt algorithms under partial shading conditions. In Proceedings of the 2016 IEEE International Conference on Power System Technology (POWERCON), Wollongong, Australia, 28 September–1 October 2016; pp. 1–6.
23. Anto, E.K.; Asumadu, J.A.; Okyere, P.Y. PID control for improving P&O-MPPT performance of a grid-connected solar PV system with Ziegler-Nichols tuning method. In Proceedings of the 2016 IEEE 11th Conference on Industrial Electronics and Applications (ICIEA), Hefei, China, 5–7 June 2016; pp. 1847–1852.
24. Abdelkader, B.; WAHID, B.A. Modeling and control of photovoltaic system using sliding mode controle, comparative studies with conventional controls. *PrzegląD Elektrotechniczny* **2020**, *96*. [CrossRef]
25. Calanca, A.; Capisani, L.; Fiorini, P. Robust Force Control of Series Elastic Actuators. *Actuators* **2014**, *3*, 182–204. [CrossRef]
26. Qi, H.; Bone, G.M.; Zhang, Y. Position Control of Pneumatic Actuators Using Three-Mode Discrete-Valued Model Predictive Control. *Actuators* **2019**, *8*, 56. [CrossRef]
27. Gong, X.; Ge, W.; Yan, J.; Zhang, Y.; Gongye, X. Review on the Development, Control Method and Application Prospect of Brake-by-Wire Actuator. *Actuators* **2020**, *9*, 15. [CrossRef]
28. Abdullaev, G.; BAKIROV, M.; Safarov, N. Silicon solar cells with antireflection layers of silicon oxide and nitride. *Appl. Sol. Energy* **1993**, *29*, 76–78.
29. Reisi, A.R.; Moradi, M.H.; Jamasb, S. Classification and comparison of maximum power point tracking techniques for photovoltaic system: A review. *Renew. Sustainable Energy Rev.* **2013**, *19*, 433–443. [CrossRef]
30. Lopez-Guede, J.M.; Ramos-Hernanz, J.A.; Zulueta, E.; Fernadez-Gamiz, U.; Oterino, F. Systematic modeling of photovoltaic modules based on artificial neural networks. *Int. J. Hydrogen Energy* **2016**, *41*, 12672–12687. [CrossRef]
31. Walker, G. Evaluating MPPT converter topologies using a MATLAB PV model. *J. Electr. Electron. Eng. Australia* **2001**, *21*, 49.
32. Hussein, K.; Muta, I.; Hoshino, T.; Osakada, M. Maximum photovoltaic power tracking: An algorithm for rapidly changing atmospheric conditions. *IEE Proc. Gener. Transm. Distrib.* **1995**, *142*, 59–64. [CrossRef]
33. Zhang, H.; Yang, X.P.; Ma, X.K.; He, B. Analysis of limit cycle behavior in DC–DC boost converters. *Nonlinear Anal. Real World Appl.* **2012**, *13*, 2049–2062. [CrossRef]
34. Asma, C.; Abdelaziz, Z.; Nadia, Z. Dual loop control of DC-DC boost converter based cascade sliding mode control. In Proceedings of the 2017 IEEE International Conference on Green Energy Conversion Systems (GECS), Hammamet, Tunisia, 23–25 March 2017; pp. 1–6.
35. Zhang, F.; Thanapalan, K.; Procter, A.; Carr, S.; Maddy, J. Adaptive hybrid maximum power point tracking method for a photovoltaic system. *IEEE Trans. Energy Convers.* **2013**, *28*, 353–360. [CrossRef]
36. Davoudi, A.; Jatskevich, J.; Chapman, P. Averaged modelling of switched-inductor cells considering conduction losses in discontinuous mode. *IET Electr. Power Appl.* **2007**, *1*, 402–406. [CrossRef]

37. Luchetta, A.; Manetti, S.; Piccirilli, M.C.; Reatti, A.; Kazimierczuk, M.K. Comparison of DCM operated PWM DC-DC converter modelling methods including the effects of parasitic components on duty ratio constraint. In Proceedings of the 2015 IEEE 15th International Conference on Environment and Electrical Engineering (EEEIC), Rome, Italy, 10–13 June 2015; pp. 766–771.
38. Locorotondo, E.; Pugi, L.; Corti, F.; Becchi, L.; Grasso, F. Analytical Model of Power MOSFET Switching Losses due to Parasitic Components. In Proceedings of the 2019 IEEE 5th International forum on Research and Technology for Society and Industry (RTSI), lorence, Italy, 9–12 September 2019; pp. 331–336.
39. Reatti, A.; Corti, F.; Tesi, A.; Torlai, A.; Kazimierczuk, M.K. Effect of Parasitic Components on Dynamic Performance of Power Stages of DC-DC PWM Buck and Boost Converters in CCM. In Proceedings of the 2019 IEEE International Symposium on Circuits and Systems (ISCAS), Sapporo, Japan, 26–29 May 2019; pp. 1–5.